The highly surprising behaviour of diphosphine ligands in iron-catalysed Negishi cross-coupling

Antonis M. Messinis,[1] Stephen L. J. Luckham,[1] Peter P. Wells,[2,3,4] Diego Gianolio,[3] Emma K. Gibson,[4,5] Harry M. O'Brien,[1] Hazel A. Sparkes,[1] Sean A. Davis,[1] June Callison,[4,6] David Elorriaga,[1] Oscar Hernandez-Fajardo,[1] Robin B. Bedford,[1]*

1. School of Chemistry, University of Bristol, Cantock's Close, Bristol, BS8 1TS, U.K.

2. School of Chemistry, University of Southampton, Highfield, Southampton SO17 1BJ, U.K.

3. Diamond Light Source, Harwell Science and Innovation Campus, Chilton, Didcot OX11 0DE, U.K.

4. UK Catalysis Hub, Research Complex at Harwell, Rutherford Appleton Laboratory, Harwell Oxon, Didcot OX11 0FA, U.K.

5. School of Chemistry, Joseph Black Building, University Avenue, University of Glasgow, Glasgow, G12 8QQ, U.K.

6. Department of Chemistry, University College London, 20 Gordon Street, London WC1H 0AJ, U.K.

Abstract.

Iron-catalysed cross-coupling is undergoing explosive development, however, mechanistic understanding lags far behind synthetic methodology. Herein we find the activity of iron-diphosphine complexes in the Negishi coupling of benzyl halides is strongly dependent on the diphosphine but the ligand does not appear to be coordinated to the iron during turn-over. This was determined using time-resolved *in operando* X-ray absorption fine structure spectroscopy, employing a custom-made flow-cell and confirmed by ^{31}P NMR spectroscopy. While the diphosphine ligands tested are all able to coordinate to iron(II), in the presence of excess zinc(II), as in the catalytic reaction, they coordinate predominantly to the zinc. Furthermore, combined synthetic and kinetic investigations implicate the formation of a putative mixed Fe-Zn(dpbz) species prior to the rate-limiting step of catalysis. These unexpected findings may not only impact upon the field of iron-catalysed Negishi cross-

coupling, but potentially beyond, to the reaction catalysed by other transition metal/diphosphine complexes.

Transition-metal-catalysed cross-coupling (Figure 1) is a powerful method for the formation of new carbon-carbon bonds; by far the most widely exploited catalysts for such processes are based on palladium complexes.[1] As with all platinum group metals, palladium suffers from high cost, low natural abundance and relatively high toxicity and therefore there are increasing attempts to replace palladium with Earth-abundant metal analogues, with iron being a particularly favoured alternative.[2-4]

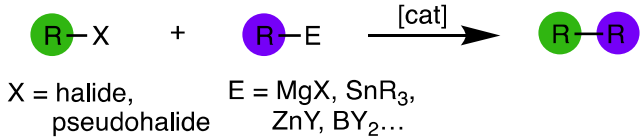

Figure 1. Generalised transition metal-catalysed cross-coupling reactions. These reactions are typically catalysed by homogeneous palladium-based catalysts.

As the range of reactions that can be catalysed by iron grows, it is becoming increasingly important to develop our mechanistic understanding in order to keep pace with progress in the field; not least to facilitate the delivery of new catalytic transformations or improve upon existent ones.[5-8] However, the paramagnetic nature of many of the catalytic intermediates, coupled with iron's propensity to undergo fast single-electron transfer (SET) processes can render such studies particularly challenging.

Iron complexes of chelating diphosphines are active pre-catalysts in a range of carbon-carbon bond forming processes,[9-28] and as such have formed the basis of a number of mechanistic studies with magnesium-,[22,24,29,30] boron-,[27,30] and zinc-based[22] coupling partners. We now report on our detailed investigations on the use of iron diphosphine complexes as pre-catalysts in a representative Negishi cross-coupling reaction with benzyl halide substrates. This study has led to some highly surprising results, not least the observation that the phosphine, while crucial for catalysis, does not appear to be coordinated to the iron during turn-over, but rather to the arylzinc reagent. Meanwhile, combined synthetic and kinetic

investigations implicate the formation of a putative mixed Fe-Zn(dpbz) species prior to the rate-limiting step of catalysis.

Results

Influence of various diphosphines on the iron-catalysed Negishi reaction.

Figure 2 shows the performance against time of iron(II) bromide with 2 equivalents of twelve different diphosphine ligands in the coupling of benzyl bromide (**1**) with Zn(4-tolyl)$_2$ (**2a**), formed *in situ* from $ZnBr_2$ and 4-tolylMgBr, giving the cross-coupled product **3**. Consistent with previously published results,[10-13,23] dpbz and dpth give excellent activity, while sciopp gave essentially identical performance to dpbz. Five other ligands (depe, MeDuphos, *cis*-dppen, dppp and iPrDuphos) performed moderately well, while dppe gave only limited activity. By contrast, the remaining three ligands – norphos, dmbz and *trans*-dppen – showed essentially no activity, giving the same profile as a control reaction with $FeBr_2$ run in the absence of phosphines (see Supplementary Figure 9). Addition of dpbz to the reaction catalysed by $FeBr_2$/*trans*-dppen initiated catalysis and then gave turn-over that mirrored the activity with $FeBr_2$/dpbz, whereas the addition of dmbz to a reaction containing dpbz led to an abrupt cessation of activity, showing that this ligand poisons the catalyst (see Supplementary Figures 24 and 22 respectively). It is clear from these results that chelating bidentate diphosphine ligands are critical for catalytic activity, and that the precise nature of the ligand can have a profound influence on catalyst performance. By contrast the use of PPh_3 gave no reaction, indicating the importance of a chelating ligand. This data, along with: (i) an examination of the effect on initial rate of reaction against changes in crystallographically-determined ligand bite angle; (ii) steric profile as measured by calculated percentage buried volume;[31] (iii) net donor properties, as judged by DFT-calculated $\nu(CO)_{symm}$ of [Ni(CO)$_2$(PP)] models[32] and (iv) the position of selected ligands on the Ligand-Knowledge Base[33] principal component maps is summarised in the Supplementary Information (Section 3). In summary, this data shows no significant trends between variation in chelating diphosphine structure and activity.

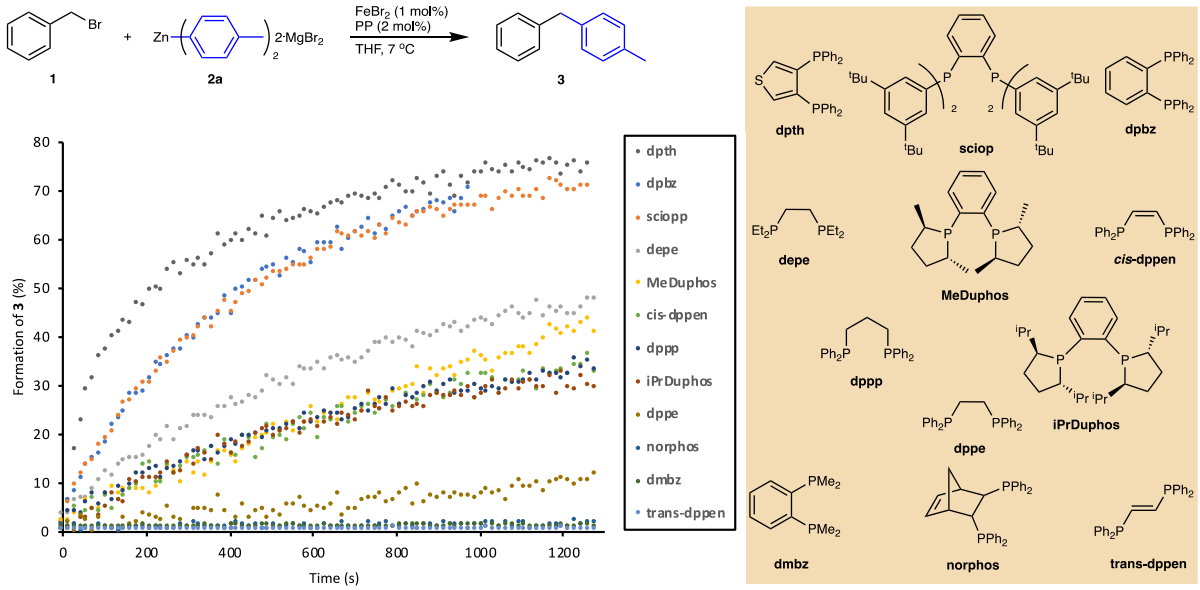

Figure 2. Activity of diphosphines in a representative iron-catalysed Negishi cross-coupling. Conditions: BnBr (**1**) (1.00 mmol), Zn(*p*-Tol)$_2$ (**2a**)/2MgBr$_2$ (1.00 mmol), diphospine (2 mol%) in THF at 7 °C, catalysis was initiated by the injection of a THF solution of $FeBr_2$ (1 mol%). Conversion to **3** was determined by *in-situ* IR spectroscopy. See Supplementary Information, section 2: Negishi cross-coupling with various diphosphines for full details.

All twelve of the diphosphine ligands investigated proved capable of forming complexes with iron(II) bromide in THF: paramagnetic peaks were observed in the ^{1}H NMR spectra of 1:1 mixtures of all of the ligands with $FeBr_2$ (spectra shown in Supplementary Methods, Section 4: Synthesis of diphosphine complexes of $FeBr_2$) except for dmbz which gave a green, highly insoluble compound (*vide infra*). Single crystal X-ray analyses of the simple 1:1 adducts [$FeBr_2$(PP)], **4**, were obtained with dpbz (**4a**), dpth (**4b**), MeDuphos (**4c**), dppp (**4d**), norphos (**4e**), *cis*-dppen (**4f**) and iPrDuPhos (**4g**). Selected examples of the structures (**4a – c**) are given in Figure 3a while those of **4d – g** are shown in Supplementary Figures 40, 42, 44 and 46 respectively. The structure of the sciopp-containing analogue has been reported previously.[34] In contrast with these mononuclear complexes, dppe gave the polymeric species [($FeBr_2$(μ^2-dppe))$_n$], **5** (Figure 3b), a result which contrasts starkly with the structure obtained for the dppp complex, **4d**. Langer and co-workers previously found that the equivalent reaction with $FeCl_2$ gave either the polymer [($FeCl_2$(μ^2-dppe))$_n$] or a mixture of this and monomeric [$FeCl_2$(dppe)$_2$], depending on the precise conditions,[35] therefore it is possible that in solution **5** exists in equilibrium with a mononuclear analogue. By contrast, the *trans*-bridging ligand

trans-dppen did not give a polymeric structure, but instead yielded the cyclic dimer [{($FeBr_2$)(μ-*trans*-dppen)}$_2$], **6** (Figure 3c).

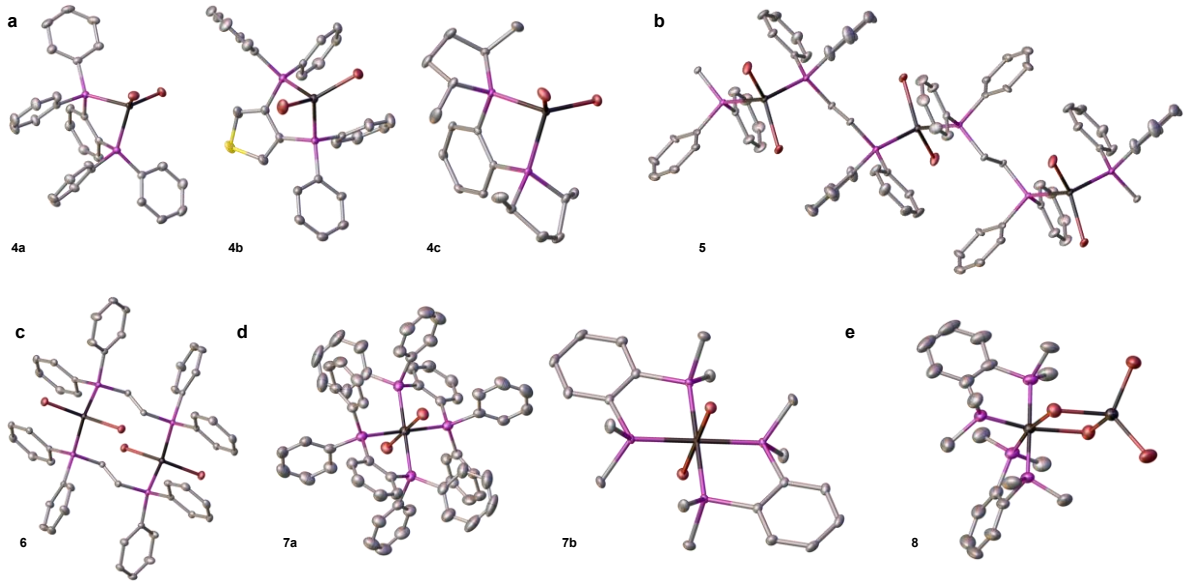

Figure 3. **Single crystal X-ray structures of $FeBr_2$-diphosphine adducts. a,** Mononuclear complexes [$FeBr_2$(PP)], PP = dpbz (**4a**), dpth (**4b**) and MeDuphos (**4c**), the structures of the analogous complexes with dppp, norphos, *cis*-dppen and iPrDuPhos (**4d – g**) are shown in Supplementary Figures 40, 42, 44 and 46 respectively. **b**, Polynuclear complex [($FeBr_2$(μ^2-dppe))$_n$], **5**. **c**, Dinuclear complex [{($FeBr_2$)(μ-*trans*-dppen)}$_2$], **6**. **d**, Bis(diphosphine) complexes [$FeBr_2$(dpbz)$_2$] (**7a**) and [$FeBr_2$(dmbz)$_2$] (**7b**). **e**, The $FeBr_2$ of **7a**, adduct [(dmbz)$_2$Fe(μ-Br)$_2$$FeBr_2$], **8**. Thermal ellipsoids set at 50% probability, hydrogen atoms and any solvents of crystallisation omitted for clarity.

Bis(diphosphine) iron(II) dibromide complexes [$FeBr_2$(PP)$_2$], **7**, can, in some cases, also be accessed: the structure of **7a** (PP = dpbz) is shown in Figure 3d and is broadly comparable with the previously reported dichloro analogue.[36] Structurally characterised examples have also been reported previously for depe[37] and *cis*-dppen.[38] Unlike with the other diphosphine-iron(II) complexes, dmbz gave a green precipitate which proved to be insoluble in all solvents investigated. Slow crystal growth by diffusion of the reactants in an H-tube (see Supplementary Methods section 4.13 for details) gave green crystals of the mononuclear complex [$FeBr_2$(dmbz)$_2$)], **7b**, along with red crystals of the non-symmetrical iron dimer [(dmbz)$_2$Fe(μ-Br)$_2$$FeBr_2$], **8**, the structures of which are shown in Figure 3d and e. The latter structure is particularly interesting as it shows that once the dmbz ligand has coordinated to

Fe(II), it is very poorly labile, even with respect to transfer to an intimately associated second Fe(II) centre.

It is clear that in most cases simple, soluble diphosphine adducts $[FeX_2(PP)_n]$ (n = 1 or 2) are readily obtained. Interestingly, the ligands that behave somewhat differently (dppe, dmbz *trans*-dppen) give iron complexes that show little or no activity in the catalysis (Figure 2), or, in the case of dmbz, actively inhibit catalysis (Supplementary Figure 22) and it is tempting to conclude that their atypical behaviour may play a significant role in this regard. However, this appears to be only part of the story, as will become apparent.

In addition to readily accessible, mono- and bis(diphosphine) Fe(II) complexes, both dpbz and dppe have previously been shown to give thermodynamically stable Fe(I) complexes of the type $[FeX(PP)_2]$ **9** (X = Cl, Br, aryl; PP = dpbz, dppe) on reaction of Fe(II) precursors with representative organozinc, -magnesium, -boron or other group 13 reagents.[22,24,26] Notably, an X-ray absorption near edge structure (XANES) spectrum of the reaction mixture of **7a** with 20 equivalent of **2a** was essentially identical to that of a sample of $[FeBr(dpbz)_2]$, **9a**, (Supplementary Figure 75; TD-DFT calculated spectrum Supplementary Figure 76). While $[FeX(dpbz)_2]$ (X = Cl, 4-tolyl) were previously excluded as potential active catalysts in Negishi cross-coupling, the pre-catalyst **9a** was shown to give comparable performance to the Fe(II) pre-catalyst, indicating that it may well be involved in catalysis.[22] Herein, we undertook a more detailed inspection and Figure 4 summarises a closer comparison of the performance of the iron(I) pre-catalyst **9a** versus the iron(II) analogue **7a** over 20 minutes.

As can be seen in Figure 4a the Fe(II) precursor initiated more rapidly and showed a higher rate of catalysis at 7 °C in THF solution. Looking more closely at the first 400 seconds of the reaction using **7a** as the pre-catalyst (Figure 4b) it can be seen that the rate of catalysis within the first 15 seconds was greater than the subsequent rate for the bulk of the reaction. This apparent 'burst phase' coincided with the formation of a small amount (~ 6%) of the iron(I) complex **9a**, however this complex cannot be responsible for the fast turn-over observed early in the reaction, but must instead be a transient side product. This is supported by examining the first 400 seconds of the reaction in which **9a** was used as a pre-catalyst (Figure 4c). During the first 9 seconds, the amount of **9a** observed rose to a maximum of around 63%. Part of this

rise may be due to stirring of the pre-catalyst into the reaction mixture, but is noticeable that this period corresponded to the rapid production of around 3% of the cross-coupled product followed by a period of inactivity of over a minute, during which time the amount of **9a** present halved. Furthermore, the amount of **9a** continued to fall after the catalytic reaction re-established, reaching <1% at 500 seconds, corresponding to only 38% conversion to the cross-coupled product **3**.

Taken together, the data in Figure 4 are consistent with the formation of a highly active, but short-lived catalytic species in the first few seconds of the reactions using both the Fe(II) and Fe(I) complexes as pre-catalyst. In order to probe the apparent speciation of the iron catalyst over time in more detail, we next undertook time-resolved X-ray absorption fine structure spectroscopic (XAFS) studies.

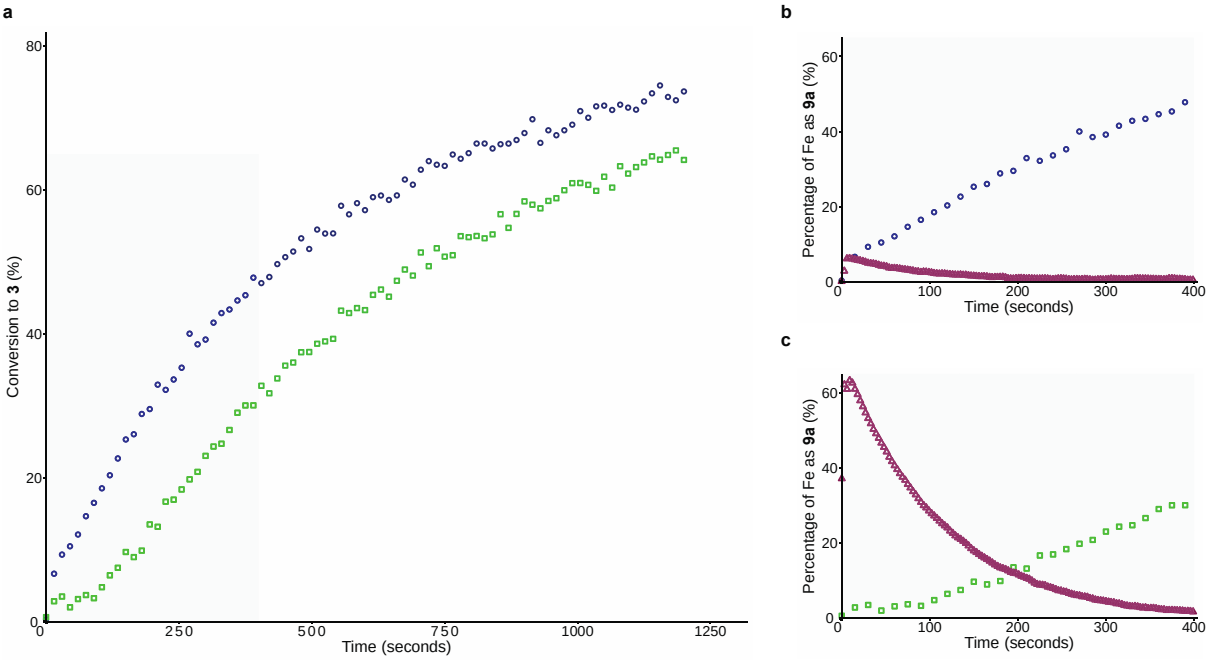

Figure 4. **Iron(I) vs. iron(II) in the Negishi coupling reaction. a**, Conversion of **1** and **2a** to **3** catalysed by [$FeBr_2(dpbz)_2$] (**7a**, ○) or [$FeBr(dpbz)_2$] (**9a**, □), determined by *in situ* IR spectroscopy. **b** and **c**, The amount of complex **9a** (△) as a percentage of total iron content against reaction progress in the couplings catalysed by **7a** and **9a** respectively (determined by *in situ* UV-vis spectroscopy), conversion to **3** included to show reaction progress.

Time-resolved X-ray absorption fine structure spectroscopy

X-ray absorption fine structure spectroscopy (XAFS) has been used previously in the investigation of potential intermediates in iron-catalysed cross-coupling reactions, however these studies focussed on either stoichiometric reactions between the iron-phosphine pre-catalysts and an appropriate nucleophilic coupling partner,[34] or on the analysis of what appears to be the end point of the catalytic reaction.[39] Similarly, XAFS has been applied to the study of the reaction of $FeCl_3$ with varying amounts of EtMgCl.[40] To gain deeper insights into the possible catalytic intermediates and their evolution throughout the course of catalysis, we undertook time-resolved XAFS, using a custom-made continuous flow reactor – which allowed us to monitor the reaction continuously at selected time-points – the details of which can be found in the Supplementary Methods section 6.2 and Supplementary Figures 67 – 69.

The catalytic coupling of **1** with **2a** was studied using the preformed iron(II) complex **7a**, at 7 °C: this complex gave identical catalytic performance when used as a pre-catalyst as the mixture of $FeBr_2$/2dpbz (see Supplementary Figure 26). Similarly, the mono-diphosphine **4a** gave the same activity as a mixture of $FeBr_2$/dpbz (see Supplementary Figure 27). Figures 5a and b show the formation of both the cross-coupled product **3** and the two homo-coupled products, 4,4'-dimethylbiphenyl (**10**) and 1,2-diphenylethane (**11**), against time in the reaction performed at 22 °C. Separately, we examined the XAFS spectrum of the bis-dpbz complex **7a** in THF solution (see Supplementary Section 6.3, Supplementary Figures 70 – 72, 74 and Supplementary Tables 6 and 7 for details) at room temperature; the data obtained for the species in solution modelled well for the mono-diphosphine complex [$FeBr_2$(dpbz)], **4a**, but poorly for the bis(diphosphine) complex **7a**, indicating that in THF loss of one of the chelating ligands is facile, an observation further supported by the ^{31}P NMR spectrum of a 1:1 mixture of **4a** and dpbz, which showed only a broadened peak corresponding to one equivalent of free dpbz (Supplementary Figure 73). ^{1}H NMR studies indicate that while **4a** is NMR active, the bis-dpbz complex **7a** is NMR silent, showing no paramagnetically shifted signals and at least 10 equivalents of dpbz need to be added to $FeBr_2$ before the signals for **4a** disappear entirely lending further support **4a** being the main species in solution when **7a** is dissolved in THF.

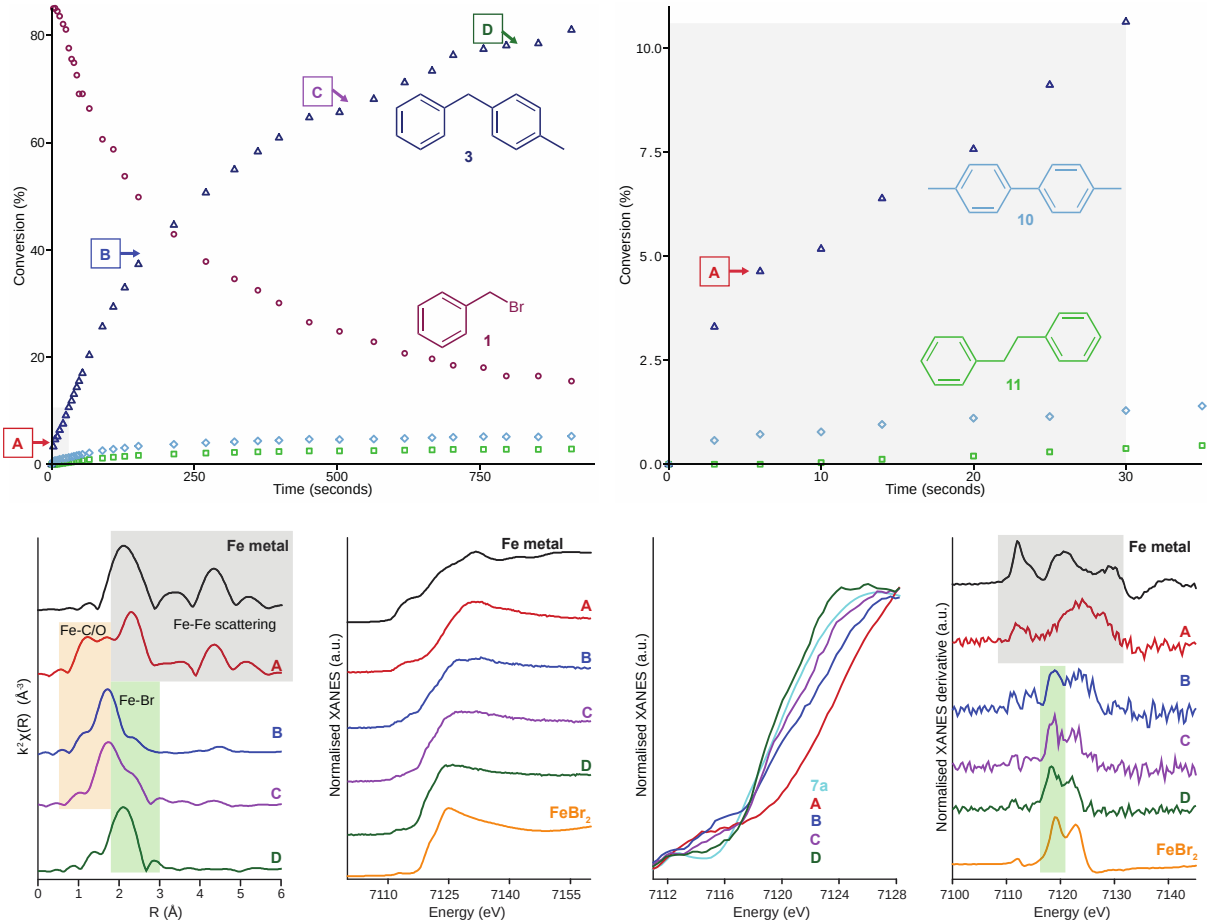

Figure 5. **Time-resolved X-ray Absorption Fine Structure spectroscopy studies. a**, Formation of cross-coupled and homo-coupled products in the coupling of **1** and **2a**, at 22 °C and the time points **A** – **D** corresponding to when XAFS data were recorded using the flow reactor (**A** = 6 s; **B** = 166 s; **C** = 482 s; **D** = 817 s). **b**, Expansion of first 30 seconds of reaction, highlighting catalytic 'burst' phase. **c**, Magnitude k^2 Fourier transform data of Fe foil and the reaction of **1** + **2**/$MgBr_2$ catalysed by [$FeBr_2$(dpbz)$_2$] (**7a**) at time points **A** – **D**. **d**, Normalised XANES spectra of Fe foil, $FeBr_2$ and positions **A** – **D**. **e**, Normalised XANES data showing close up of edge position of complex **7a** and positions **A** – **D**. **f**, Normalised XANES derivative spectra of Fe foil, $FeBr_2$ and positions **A** – **D**.

Figure 5a also highlights the time points **A** – **D** corresponding to the periods when the flow XAFS spectra were recorded (room temperature). Following the reaction profile in this way, with both the X-ray absorption near edge structure (XANES) and extended X-ray absorption fine structure (EXAFS), we observed significant and unexpected changes to the composition of the iron-containing components (Figure 5c – f, see Supplementary Figure 77 for larger versions of these plots). Probing the iron speciation directly after the 'burst phase' (point **A**: t = 6s; conversion to **3** ~5%), it is apparent that significant structural changes had already occurred. The EXAFS data (Figure 5c) indicate significant long-range ordering, with readily

identifiable scattering paths consistent with the formation of metallic Fe(0). The EXAFS data at this time are well-modelled (Supplementary Figure 78 and Supplementary Table 8) using scattering paths from metallic Fe with additional Fe-C/O scattering paths at 1.85(2) and 2.05(2) Å. By contrast, the inclusion of additional Fe-Br and Fe-P paths within the primary coordination sphere of iron gave significantly worse agreement between the experimental and simulated EXAFS data (Supplementary Figure 79 and Supplementary Table 9). We have previously shown that iron nanoparticles can be formed during the cross-coupling of aryl Grignard reagents with alkyl halides when chelating diamines are used as ligands or additives,[41] however it has been widely assumed that chelating diphosphines would prevent the formation of such nanoparticles as they are far better donors for the iron centre. The observation that metallic iron formed during the burst phase, coupled with the absence of Fe-P interactions at this time point indicate that this assumption is not valid.

As well as metallic Fe(0), the spectra indicate the presence of Fe-C/O, presumably corresponding to dissolved homogeneous complexes, formed either (a) on the way to or in competition with iron nanoparticles or (b) by dissolution of some of the nanoparticles on reaction with the substrate **1**, a process we have observed previously.[42] EXAFS is unable to distinguish between neighbours of similar atomic number and cannot therefore directly distinguish between Fe-O (e.g. coordinated THF) and Fe-C (aryl or benzyl complexes). Considering likely carbon-based contenders for the two distinct scatterers, typical Fe-C(aryl) bonds range between 1.96 and 2.08 Å for Fe(II) and Fe(I) aryl complexes,[26,43-46] and are around 1.93 Å for iron(III) aryls.[47] Meanwhile, the Fe-C bond lengths in structurally characterised Fe-benzyl complexes typically range from 2.04 – 2.12 Å.[42,48] The most likely oxygen donor is THF, and the longer of the two iron-scatterer distances falls within the range reported for Fe(II) and Fe(III) THF adducts,[49-52] but is significantly shorter than the Fe-O distance reported for THF coordinated to (formally) Fe(I) centres.[53-55] Summarising, the shorter distance most likely corresponds to an Fe-aryl while the longer could reasonably be due to Fe-aryl, Fe-benzyl or Fe-THF bonds.

Clearly the EXAFS data do not allow us to distinguish between Fe-C/O on iron in a variety of oxidation states from Fe(I) – Fe(III). The XANES spectrum recorded at point **A** shows a shift of the main edge to higher energy compared with the spectrum of the pre-catalyst

[$FeBr_2(dpbz)_2$], **7a**, and there is a broad pre-edge feature centred at 7115 eV. A shift to higher energy is commonly associated with a change in oxidation state however, in this instance, it may instead be correlated to a loss of halide. Previous studies have shown the first row transition metal halides have apparent edge positions much lower than expected as a result of transitions to *p*-orbitals arising from the coordinated ligand.[56] A comparison of the XANES spectra of $FeBr_3$ and Fe_2O_3 (Supplementary Figure 80) shows an approximately 5 eV shift in edge position, confirming this is also the case for systems with bromide coordinated to iron. The broad nature of the pre-edge feature observed at 7115 eV is characteristic of Fe metal and supports the conclusions based on the EXAFS data.

At point **B** (t = 166s; conversion to **3** ~ 39%) the EXAFS spectrum (Figure 5c) shows a significant loss of metallic structure. Meanwhile the XANES spectrum confirmed the presence of bromide neighbours by a shift of the main edge to lower energy (Figure 5e); the derivative of the XANES spectrum (Figure 5f) shows a peak at 7119 eV, which is also readily apparent in the reference spectrum of $FeBr_2$. A simulation of the EXAFS data (Supplementary Figure 78 and Supplementary Table 8) at time point **B** was achieved by a fitting model incorporating three scattering paths: two Fe-C/O and one Fe-Br. By time point **C** (t = 482 s; conversion to **3** ~ 65%) there was a reduction in Fe-C/O scattering interactions, whilst Fe-Br scattering events increased; by point **D** (t = 817s, yield **3** ~ 78%) the EXAFS data can be modelled with a primary coordination sphere consisting solely of bromide ligands (Supplementary Figure 78 and Supplementary Table 8; see below for further details of the proposed dimeric iron bromide structure). The absence of any Fe-O interactions is suggestive of a bromoferrate anion lacking coordinated THF ligands (*vide infra*).

Summarising, the early burst phase of catalysis corresponds with the formation of iron nanoparticles. While these may serve as a short-lived but highly active catalyst, they may equally represent the decomposition of a very short-lived, highly active homogeneous species. Even by this early time point there is clear evidence for the presence of Fe-C/O species that persist through the majority of the main phase of catalytic turn-over. By contrast there is no evidence for any Fe-Br species at this early stage, however, these are present at all later stages and represent the principal component of the reaction mixture by the twilight phase of catalysis. Astonishingly, within the resolution of the technique, there is no evidence

for any significant coordination of the diphosphine ligand, dpbz, to iron during any phase of the catalysis. This highly surprising result clearly raises two major questions: where is the dpbz during the catalysis and, given that it is essential for catalytic activity, what is its role?

Phosphine-zinc species

In answer to the first question posed above, it is highly likely that dpbz, and the other diphosphine ligands tested, coordinate to Zn(II); either the $Zn(tolyl)_2$ present at the outset of catalysis or the ZnBr(tolyl) and $ZnBr_2$ formed as the reaction progresses. All of the diphosphines reacted with $ZnBr_2$ in a 1:1 ratio as judged by ^{31}P and ^{1}H NMR spectroscopy (see Supplementary Methods, section 7). Single crystal X-ray structures of the mononuclear complexes $[ZnBr_2(PP)]$, **12**, were obtained with dpbz, dpth, sciopp, iPrDuphos, *cis*-dppen, dppp, norphos and dmbz (**12a** – **h** respectively); representative examples (**12a** and **b**) are shown in Figure 6a, while the remaining six are given in Supplementary Figures 91, 95, 99, 103, 107 and 111 respectively. As with the iron complexes above, *trans*-dppen gave a dinuclear complex with zinc bromide $[\{ZnBr_2(\mu\text{-}trans\text{-dppen})\}_2]$, **13** (Figure 6b). Meanwhile, as observed with iron(II), dppe has previously been shown to give the polymeric Zn(II) complex $[\{ZnBr_2(\mu\text{-dppe})\}_n]$, **14**.[57] In addition to these zinc bromide complexes, arylzinc complexes with diphosphine ligands were readily formed, with monomeric complexes represented by the monoaryl complex [ZnBr(4-tol)(dpbz)] (**15**, Figure 6c) and the diaryl complexes $[Zn(Ar)_2(PP)]$ **16** (**16a**, PP = dpbz, Ar = 4-tolyl and **16b**, PP = *cis*-dppen, Ar = 4-tolyl shown in Figure 6c; **16c**, PP = dppp, Ar = Ph shown in Supplementary Figure 137). Meanwhile, and in line with the results obtained above with Fe(II), dppe showed a propensity for polymer rather than monomer formation, as illustrated by the structure of $[\{ZnPh_2(\mu^2\text{-dppe})\}_n]$ **17** (Figure 6d).

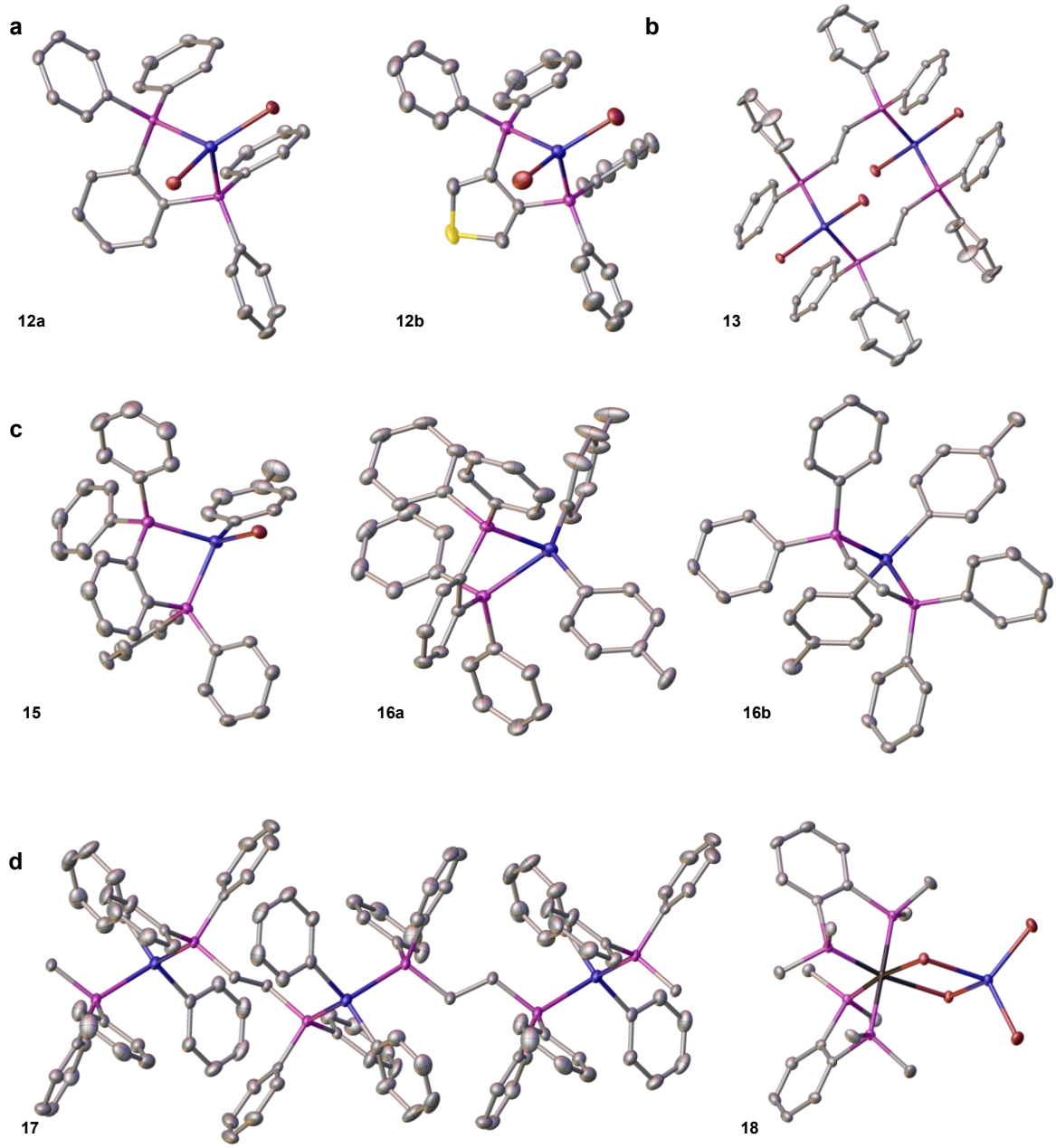

Figure 6. Single crystal X-ray structures of Zn(II)-diphosphine adducts. a, Mononuclear complexes [$ZnBr_2$(PP)], PP = dpbz (**12a**) and dpth (**12b**). Analaogous structures with sciopp (**12c**); iPrDuPhos (**12d**); *cis*-dppen (**12e**); dppp (**12f**); norphos (**12g**) and dmbz (**12h**) are shown in Supplementary Figures 91, 95, 99, 103, 107 and 111 respectively. **b**, Dinuclear complex [{$ZnBr_2$(μ-*trans*-dppen)}$_2$], **13**. **c**, Diphosphine monorarylzinc adduct [ZnBr(4-tolyl)(dpbz)] (**15**) and diarylzinc adducts [Zn(Ar)$_2$(PP)] **16a** (PP = dpbz, Ar = 4-tolyl) and **16b** (PP = *cis*-dppen, Ar = 4-tolyl); analogous structure of **16c** (PP = dppp, Ar = Ph) is shown in Supplementary Figure 137. **d**, Polymeric diarylzinc adduct [{$ZnPh_2$(μ^2-dppe)}$_n$] **17**. **e**, Mixed Fe-Zn complex [(dmbz)$_2$Fe(μ-Br)$_2$$ZnBr_2$], **18**. Thermal ellipsoids set at 50% probability, hydrogen atoms and any solvents of crystallisations omitted for clarity.

While it is clear that Zn(II) readily complexes with the diphosphines used in the catalysis, this does not necessarily mean that such Zn-phosphine adducts are formed in the presence of

iron. In all cases (except dmbz, which gives insoluble iron complexes) we examined the competition reactions of the [$FeBr_2$(PP)] complexes with 5 – 80 equivalents of $ZnBr_2$ by ^{1}H and ^{31}P NMR spectroscopy. In the cases of dpbz, sciopp, iPrDuphos, MeDuPhos *cis*-dppen, dppe, dppp and *trans*-dppen we were able to delineate the proportion of the ligand on the zinc(II) (see Supplementary Methods, section 8), which by 80 equivalents of $ZnBr_2$ fell in the range 88 – 100%. Interestingly, in the case of [$FeBr_2$(dmbz)$_2$], slow crystallisation in the presence of $ZnBr_2$ led to the formation of highly insoluble [(dmbz)$_2$Fe(μ-Br)$_2$$ZnBr_2$], **18**, the structure of which is given in Figure 6d. As with [(dmbz)$_2$Fe(μ-Br)$_2$$FeBr_2$], this suggests a lack of migratory aptitude of the dmbz ligands from the Fe(II) to the Zn(II) centre.

In the case of dpbz with only 5 equivalents of $ZnBr_2$, the equilibrium between the diphosphine coordinated to the zinc(II) versus coordination to one or more Fe(II) species lay in favour of the latter, with only around 25% of the ligand coordinated to the zinc. This is mirrored by a DFT calculation (B3LYP-D3/6-311+G*//B3LYP-D3/6-31G*/SDD, details in Supplementary Methods, section 9) of the exchange of the dbpz ligand between [$FeBr_2$(dpbz)] (**4a**) and [$ZnBr_2$(THF)$_2$] to give [$ZnBr_2$(dpbz)] (**12a**) and [$FeBr_2$(THF)$_2$]. This showed the process to be mildly endergonic (ΔG = +0.5 kcal/mol), which corresponds to a calculated equilibrium constant, *K*, of around 0.4 at 298 K, a value broadly consistent with the spectroscopic data. At the start of the catalytic reaction, the Zn(II) is in the form of a diarylzinc reagent rather than $ZnBr_2$, however it was not possible to directly measure dpbz equilibration between iron and zinc in this case due to subsequent transmetallation processes. Accordingly, we probed computationally the dpbz exchange between **4a** and [$ZnPh_2$(THF)$_2$], giving [$ZnPh_2$(dpbz)] (**16a'**) and [$FeBr_2$(THF)$_2$]. This gave a very similar result to that with zinc bromide, with a calculated ΔG = +1.0 kcal/mol, corresponding to a *K* of about 0.2 at 298 K.

Next, we probed dpbz-complex speciation during catalysis using ^{31}P NMR spectroscopy (see Supporting Information, section 10 for full details). The low concentration of dpbz and broad nature of Zn(PP) peaks in the mixture (*vide infra*) in the catalytic reaction meant that satisfactory data could not be recorded in less than 5 minutes, even with the relatively fast spin-lattice (T_1) relaxation recorded for dpbz under these conditions. This means that each ^{31}P spectrum corresponds to a 'time-window', with the data obtained representing a time-

average of species that may not be present over the whole window. Two ^{31}P NMR spectra were recorded at 3 – 8 minutes (time-window 1) and 9 - 14 minutes (time-window 2) while single scan ^{1}H NMR spectra were recorded immediately before and after each, giving the conversion to cross-coupled product **3** during the time-windows. Time-windows 1 and 2 corresponded to 25 – 50% and 50 – 63% conversion to **3** respectively. During both time-windows a single broad peak was observed at -18 ppm (FWH ~ 160 Hz) consistent with the coordination of dpbz to one or more Zn(II) centres. The broad nature of the peak – presumably due to rapid exchange, paramagnetic broadening by Fe species present, or both – preclude definitive identification of the exact (dpbz)Zn(II) species. Repeated attempts to quantify the amount of (dpbz)Zn(II) by using a fast-relaxing internal standard ([$NiCl_2$(dppe)], see Supplementary Information section 10 for full details) proved fruitless for spectra recorded at time-windows 1 and 2, however the observation of a single broad peak throughout turn-over meant that we were able to repeat the reaction monitoring with a much broader time-window (0 – 40 minutes, 0 – 87% conversion to **3**). This showed that essentially all of the dpbz was coordinated to Zn(II) during the bulk of turn-over.

Taken together, the data indicate that not only can the diphosphine coordinate to Zn(II), but that under catalytically relevant conditions (large excess of Zn(II)) the majority, if not all of the ligand is coordinated to the zinc. This is not only consistent with the NMR spectroscopic data, but also with the absence of any observable Fe-P in the time-resolved XAFS studies. We note that iron is essential for activity, precluding the possibility that catalysis proceeds via a zinc-mediated process.[58] Furthermore, a comparison of reactivity under conditions that allow the zinc-mediated process in both the presence and absence of dpbz showed that the diphosphine retards the rate (Supplementary Figure 162). What then is the role of the phosphine? One possibility is that by coordinating to the diarylzinc reagent, the dpbz may facilitate transmetallation, accordingly we next explored this possibility in detail.

Examining transmetallation

We explored transmetallation of the aryl group from zinc to iron, with and without the diphosphine ligand, dpbz. Two different diarylzinc reagents were used, **2a**, and $Zn(mes)_2$, **2b** – the former chosen as it directly mirrors the behaviour in the catalytic reaction, the latter as it produces kinetically-stable iron complexes that can readily be explored by paramagnetic ^{1}H

NMR spectroscopy. The arylzinc reagents used in iron-catalysed Negishi cross-coupling are typically prepared, *in situ*, by reaction of an appropriate zinc halide with a Grignard reagent.[11-13,22,24] We have previously shown that residual magnesium salts in the zinc reagents are essential for activity: when the aryl zinc compounds are instead prepared from aryl lithium reagents, no activity is observed, however catalysis can be restored by the addition of MgX_2.[11] We previously speculated that the role of the magnesium salts may be to furnish triarylzincate nucleophiles, $[MgX][Zn(aryl)_3]$, **19**, *via* a hetero-Schlenk equilibrium. Such zincates might reasonably be expected to undergo far more facile transmetallation processes with the iron catalyst than diarylzinc species. However, the results of the catalytic reaction outlined in Supplementary Figure 174 clearly indicate that such triarylzincates cannot be the major zinc-based nucleophiles in the cross-coupling. Here, the homocoupling reactions of both the nucleophile **19a** (aryl = 4-toyl) and the electrophile **1** far outstrip the cross-coupling reaction when the zincate is exploited as the nucleophile.

To probe further the role of both $MgBr_2$ and any $ZnBr_2$ present, we investigated the reactions of $FeBr_2$ with magnesium-free **2a**, prepared from 4-tolyllithium, under varying conditions (Figure 7). The reaction in the absence of any added salts at room temperature (Figure 7a) gave a yellow solution which within minutes started to darken, giving a black, magnetic precipitate of iron nanoparticles that could easily be separated by magnetic entrainment. TEM analysis of the particles (for full details see Supplementary Methods section 11.1.5 and Supplementary Figures 177 - 183) showed polydisperse, electron-dense particles with diameters typically ranging from 100 to 600 nm. EDX analysis revealed the presence of Fe, Zn, Br and I (presumably from the 4-tolyiodide used to prepare the aryllithium reagent that was in turn used to prepare the Mg-free **2a**). TEM of a water-washed sample (Figure 7a) revealed particles with similar dimensions to the unwashed samples. Generally there was less background material and the sub-micron particles were clearly nanostructured, possibly as aggregates of crystalline nanoparticles (5-10 nm in diameter). EDX analysis indicated the sample contained predominantly Fe along with Zn, trace Br and negligible I (Supplementary Figure 178). Elemental mapping confirmed the particles were composed of Fe with both Zn and the trace Br signals closely associated with the particles (Supplementary Figure 179).

This reaction was accompanied by the formation of 4,4'-bitolyl (**10**), the production of which against time is shown in Supplementary Figure 184. Within 20 minutes, around 21% of the Fe(II) had been reduced to Fe(0), while by 7 hours this had risen to 57%. This clearly demonstrates that transmetallation of the aryl group from the diarylzinc reagent to the iron, followed by reductive elimination of the biaryl and formation of Fe(0) are facile processes. It is important to note that the results from this reaction correspond well with the formation of metallic iron in the 'burst phase' of the catalysis described above, as observed by time-resolved XAFS.

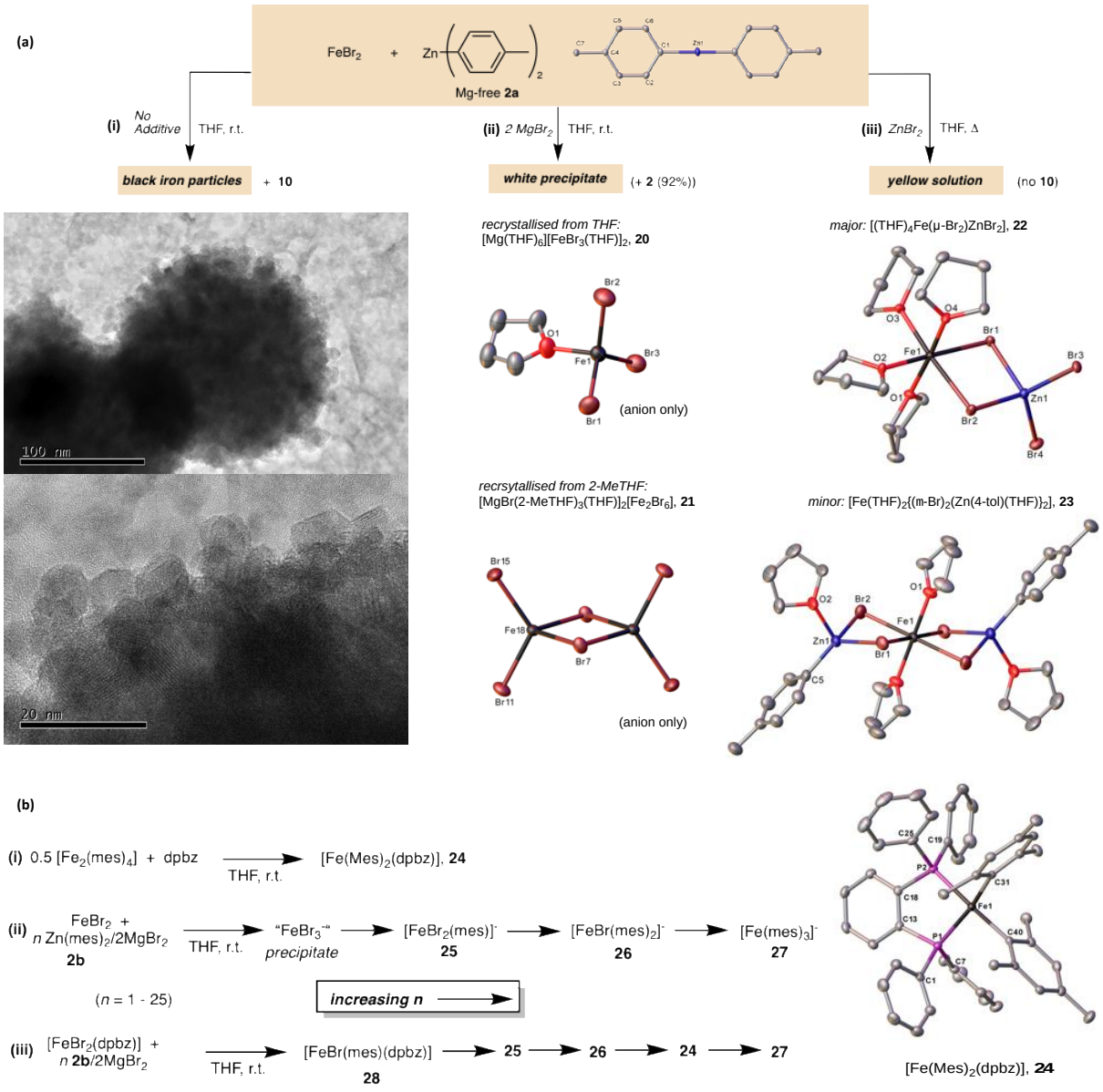

Figure 7. Transmetallation Studies. (a) Effect of salt additives on the reactions of $FeBr_2$ with 2 and **(b)** transmetallation studies with kinetically stabilised mesityl-containing intermediates. **a(i)**, No additive in THF at room temperature and TEM images of the magnetic iron(0) particles produced. **(ii)**, 2 Equivalents of $MgBr_2$ in THF at room temperature and the crystal structures

of the resultant anionic complexes **20** and **21** (counterions omitted for clarity) crystallised from THF and 2-MeTHF respectively. **(iii)**, $ZnBr_2$ at reflux in THF and crystal structures of the complexes **22** and **23** from crystals grown from the reaction mixture. The crystal structure of magnesium-free **2a** is also shown at the top of the figure. In all cases, the thermal ellipsoids are set at 50% probability, H-atoms and any solvents of crystallisation omitted for clarity. **b(i)** formation and crystal structure of **24**, **b(ii)** and **(iii)** transmetallation sequences with mesitylzinc in absence and presence of dpbz respectively.

By contrast, when the reaction was repeated in the presence of added magnesium bromide (Figure 7b), as would be the case in the catalytic reactions, then no transmetallation was observed. Instead the diarylzinc reagent was recovered in high yield, and a white, highly air-sensitive precipitate was obtained. This precipitate was recrystallised from both THF and 2-MeTHF, and in both instances bromoferrate complexes were obtained. In the former case, this consisted of a THF adduct of $FeBr_3^-$ (**20**), while in the latter the homoleptic dimer $[Fe_2Br_6]^{2-}$ (**21**) was obtained. Modelling the EXAFS data recorded at point **D** (*vide supra*) gave a good fit with the structural data obtained for **21**, with two distinct Fe-Br scattering paths containing Fe-Br separations of 2.33(5) and 2.45(3) Å for the bridging and terminal bromides respectively, consistent with the crystallographic data. The mean square disorder parameter, σ^2, for the bridging Fe-Br distance has a smaller value than would normally be expected, however, this can be accounted for by the rigid structure afforded by the dimeric form of the anion. After standing for 2 days, some formation of Fe(0) was apparent; leaving for a week gave substantial formation of magnetic, zerovalent iron powder. Meanwhile, rapid formation of Fe(0) could be triggered by heating the reaction mixture to reflux temperature. It seems that the formation of these bromoferrate species actively inhibits transmetallation from the zinc to the iron centres at low Fe:Zn ratios, with somewhat forcing conditions required to overcome this inhibition.

Is the inhibition of transmetallation due simply to the presence of the negative charges on the iron centres? The reaction outlined in Figure 7c suggests the answer to this question is no. Here, the reaction of $FeBr_2$ and magnesium-free **2a** was conducted in the presence of $ZnBr_2$, a salt that would be produced during the course of the catalytic reaction. In this case, a yellow solution was obtained which proved to be stable with respect to formation of iron(0), even when heated at reflux temperature for several hours. Crystals grown from the reaction mixture comprised of two distinct species, the major one being the zinc bromide adduct of

an iron dibromide (**22**). On the other hand, the minor species proved to be an arylzinc adduct of a neutral iron dibromide (**23**). Such arylzinc-transition metal adducts are very rare,[59-61] and its formation and stability with respect to decomposition to Fe(0), even under forcing conditions, demonstrates that transmetallation from the zinc to *neutral*, let alone anionic iron centres is not at all facile.

How then does transmetallation occur in the catalytic reaction, particularly under such mild conditions? To probe this, two equivalents of dpbz were added to the suspension of the white precipitate obtained according to Figure 7a(ii) using **2a** (prepared *in situ* from the Grignard). This led to the rapid production of a dark red solution of the Fe(I) complex **9a**, which was obtained in essentially quantitative spectroscopic yield (determined by UV-Vis spectroscopy, see Supplementary Methods, section 11.1.8.2). We have previously shown that **9a** results from transmetallation followed by reductive elimination, demonstrating unequivocally that addition of the diphosphine facilitates transmetallation. Similar results were obtained, if the dpbz was first stirred with the **2a** in THF to generate **16a** *in situ*, and then $FeBr_2$ added (see Supplementary Methods, section 11.1.8.2 for details). Meanwhile, when a yellow solution prepared according to the method in Figure 7a(iii) was reacted with two equivalents of dpbz per Fe at reflux for 30 minutes and then left to stand for 4 days, a mixture of crystals was obtained comprised of **9a**, [$FeBr_2$(dpbz)] (**4a**) and [ZnBr(4-tol)(dpbz)] (**15a**) (Supplementary Methods, section 11.1.8.3.2).

Taken together with the absence of Fe-P species during catalysis, as determined by the time-resolved XAFS (*vide supra*), these data suggest that transmetallation may be accelerated by coordination of dpbz, either to the Zn(II) centre, or by transient coordination to Fe(II). To probe this further, we turned next to the sterically hindered reagent $Zn(mes)_2$, **2b**. Interestingly, we found that **2b** does not react with dpbz, presumably due to the steric hindrance of the bulky mesityl groups whereas [{$Fe(mes)_2$}$_2$] does (Figure 7(b)(i)), giving the mononuclear adduct [$Fe(mes)_2$(dpbz)], **24**, the structure of which is shown in Figure 7(b). Complex **24** is stable in solution at room temperature, highlighting the kinetic stability introduced by the use of the bulky aryl residues. The lack of coordination of dpbz to **2b** allowed us to isolate the effect on transmetallation of coordination of the diphosphine to the iron, rather than to zinc.

The reaction of $FeBr_2$ with increasing amounts of **2b**/2$MgBr_2$ was followed by ^{1}H NMR spectroscopy; as with the smaller diarylzinc reagent **2a**, in the presence of $MgBr_2$, addition of one equivalent of the mixture led to the formation of a white precipitate – presumably the same bromoferrates as observed with **2a**/2$MgBr_2$ – which remained with up to 3 equivalents of added **2b**/2$MgBr_2$. By four equivalents, the precipitate had dissolved and paramagnetically-shifted peaks for two new species were observed in the ^{1}H NMR spectrum, assigned to the heteroleptic ferrate anions, $[FeBr_2(mes)]^-$ (**25**) and $[FeBr(mes)_2]^-$ (**26**) as the sole paramagnetic species (see Supplementary Information section 11.2.3 for full details). Complex **26** was also obtained on reaction of $[\{Fe(mes)_2\}_2]$ with $[NBu_4]Br$. By ten equivalents of **2b**/2$MgBr_2$, the mono-aryl 'ate' complex **25** was absent, with the mixture comprising of **26** (minor species) and the known homoleptic ferrate $[Fe(mes)_3]^-$ **27** (major species). By 25 equivalents, **27** was the predominant species, although a trace amount of **26** was still apparent. Figure 7(b)(ii) summarises the order of formation of the observed ferrate species.

Repeating the reaction, but with $[FeBr_2(dpbz)]$, **4a**, in place of $FeBr_2$ showed that between 1 and 3 equivalents of **2b**/$MgBr_2$ an increasing amount of [FeBr(mes)(dpbz)], **28**, was observed alongside **4a** (see Supplementary Information, section 11.2.6 for details). By four equivalents, the reaction mixture comprised of **28** and a small amount of the heteroleptic monoaryl 'ate' complex, **25**. More **25** was observed at 5 equiv. along with the bis-aryl diphosphine adduct **24**. The appearance of some of the phosphine-free ferrate intermediate **25**, prior to the observation of the bis-mesityl dpbz adduct **24** is noteworthy, suggesting the ferrate may form directly from either **4a** or possibly **28**. At 5 equivalents, the spectrum reveals a mixture of **28**, **24** and **26**, while by 25 equivalents, the sole observable paramagnetic species was the homoleptic ferrate, **27**. Monitoring the addition by ^{31}P NMR spectroscopy revealed the presence of a peak at –17.3 ppm, which we tentatively assign to the formation of [ZnBr(mes)(dpbz)], **15b** (see Supplementary Methods, sections 11.2.6 and 11.2.5 for details), as the transmetallation progressed, along with a second peak at 35.4 ppm, which grew in and then reduced, disappearing by 25 equivalents. As yet we have been unable to assign this second peak, but note that it is too far down-field to be coordinated to a simple Zn(II) centre and is too sharp to be coordinated to a paramagnetic iron centre. It is possible that it may be

coordinated to a Zn(II) centre which is in turn coordinated to an Fe centre via bridging bromides (*vide infra*).

From these transmetallation studies, the following can be concluded. Firstly, when the ratio of $Zn(aryl)_2/2MgBr_2$ to $FeBr_2$ is low, no transmetallation occurs, instead bromoferrate anions are precipitated. Increasing the relative amount of the zinc reagent, to levels more representative of the catalytic reaction, leads to the production of soluble hetero- and then homoleptic organoferrates. When the reaction is repeated in the presence of dpbz, then no precipitation occurs, and instead first mono and then bis-aryl iron diphosphine intermediates are formed. However, as the amount of diarylzinc is increased to levels more representative of catalysis, again the homoleptic, phosphine-free organoferrate is the predominant iron species. Thus, while dpbz on the iron centre certainly facilitates transmetallation at lower Zn loadings, this is not relevant under catalytic conditions. Finally, it should be noted that while the mesityl ligand is useful for kinetically stabilising models of potential catalytic intermediates, no activity was seen in an attempted coupling of $Zn(mes)_2$ with **1**, even under forcing conditions (see Supplementary Information, section 11.2.7).

Kinetic Studies

Finally we undertook a kinetic investigation of the post 'burst-phase' manifold for the coupling of **1** with **2a**. The data from this (see Supplementary Methods section 12 and Supplementary Figures 200 – 231 for full details) yielded the rate equation (1):

$$d[\mathbf{3}]/dt = k[FeBr_2]^{1.4}[dpbz]^{x}[\mathbf{1}]^{0}[\mathbf{2a}]^{0} \quad (1)$$

where x = 1.4 with up to 2 equivalents of dpbz added per iron, and zero order above this point. The greater than first order dependence on [Fe] is consistent with the rate-limiting process involving the slow reaction between two discrete iron species; the fractional order indicates that the reaction manifold is complex. Furthermore the zero-order dependence on *both* substrates indicates that the activation of either substrate at iron is not part of the rate-limiting process.

It is tempting to conclude that the dependency of the rate on [dpbz] at dpbz:Fe ratios of less than two, and the lack of dependency above this ratio, is due to a competition between Fe and Zn for coordination of dpbz, but this is inconsistent with the dpbz-Zn-Fe speciation studies above which show that this equilibrium will lie heavily in favour of coordination to the zinc(II) under the catalytic conditions. Conversely, if all that were required is coordination of the dpbz to Zn to accelerate the rate-limiting process, then there should be a positive order dependence on dpbz at all loadings, which is clearly not the case, instead the reaction saturates at a somewhat telling dpbz:Fe ratio of 2 : 1.

Discussion and A Plausible Mechanism

In our attempts to deconvolute the large amount of data obtained in this study, we believe the following are perhaps the most salient observations: (i) both time-resolved XAFS and ^{31}P NMR spectroscopic studies show that during catalytic turn-over essentially all of the chelating bisphosphine is coordinated to Zn(II), not iron; (ii) reaction of Fe(II) precursors with excess diaryzinc reagents give homoleptic arylferrates, consistent with the Fe-C species observed during turn-over by time-resolved XAFS; (iii) the formation of these organoferrates occurs irrespective of the presence or absence of the diphosphine ligand, yet the ligand is essential for catalytic activity – the formation of the organoferrates cannot by itself account for activity; (iv) the rate of catalysis is dependent on the concentration of dpbz, up to a dpbz:Fe ratio of 2, and independent of the phosphine concentration above this point, yet under catalytic conditions (50 equiv. of Zn(II)) the amount of Fe(dpbz) adducts would be negligible; (v) the rate of catalysis is 1.4 order in [Fe] and (vi) neither substrate appears in the rate equation for catalysis. Any mechanistic proposal must account for all of these observations.

Figure 8 outlines schematically our current tentative working hypothesis for the role of the diphosphine which is consistent with all the observed data obtained from the time-resolved spectroscopic investigations of the catalytic reaction, the stoichiometric investigations of the transmetallation process and the kinetic data of the catalytic reaction. In the proposed scenario, diarylzinc reacts with an iron(II) halide intermediate to generate the putative intermediate ***I₁***. The reaction of ***I₁*** with the chelating diphosphine gives a second postulated intermediate ***I₂*** in which the diphosphine ligand has coordinated to the zinc centre. Both ***I₁*** and ***I₂*** may be trimetallic Zn-Fe-Zn species as this would be consistent with both the X-ray

crystal structure of the complex **23**, which is closely related to the proposed intermediate ***I*$_1$**, and the observed saturation in the rate of catalysis at a Fe:dpbz ratio of 1:2 – the ratio necessary to give a '(dpbz)Zn-Fe-Zn(dpbz)' adduct. In this scenario, the rate-determining step in the catalytic reaction is proposed to occur after the reaction of intermediate ***I*$_2$** with a benzyl-iron intermediate, formed elsewhere in the manifold. This would account for the rate of catalysis being independent of the concentration of either substrate and having a greater than first-order dependence on the concentration of iron.

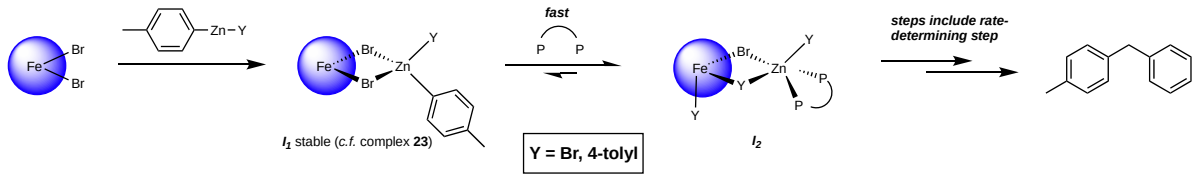

Figure 8. Schematic of a tentative suggestion for the role of chelating diphosphine in the catalytic reaction. In the proposed mechanism, the inactive intermediate ***I*$_1$** , closely related to the isolated complex **23**, reacts with a chelating diphosphine (P~P) to give the active intermediate ***I*$_2$**; the rate-determining step occurs subsequently.

The formulations of intermediates ***I*$_1$** and ***I*$_2$** are consistent with the lack of direct Fe-P interactions in the time-resolved XAFS studies. The observation of Fe-C species in the time-resolved XAFS may reflect Fe-aryl or benzyl moieties in either of the intermediates ***I*$_1$** or ***I*$_2$**. While a simple iron-4-tolyl complex would not be expected to be stable under the reaction conditions,[42] coordination of one or two zinc bromide-containing fragments to the iron may well lead to enhance kinetic stability, accounting for the observation of abundant Fe-C species by XAFS.

The lack of activity in the absence of a chelating diphosphine is consistent with intermediate ***I*$_1$** not itself being catalytically competent, rather activity being 'switched on' by coordination of the phosphine to the Zn(II). It is not possible, at this stage, to determine what specific process is accelerated by the putative coordination of the diphosphine to the zinc, but it does appear that this process is crucial for activity.

Conclusions

In summary, we have exploited time-resolved flow XAFS spectroscopy to study catalyst speciation during a representative iron-catalysed Negishi cross-coupling reaction. We found that a rapid 'burst phase' is followed by a period of slower catalysis that accounts for the majority of product formation. The burst phase is marked by the formation of metallic iron,

but we cannot at this stage say whether the catalyst here is homogeneous or heterogeneous. Meanwhile, during the main turn-over period the iron is predominantly in the form of homo or heteroleptic organoiron complexes, followed by the formation of increasing amounts of iron bromide complexes, most likely in the form of bromoferrates, until by the end of the reaction these are the predominant species. Despite being vital for catalytic activity, the diphosphine ligand is not, to any observable extent, coordinated directly to the iron during turn-over. Instead, the phosphine coordinates predominantly to Zn(II) under the reaction conditions. We propose that coordination of the diphosphine to the zinc centre of an Fe-Zn intermediate is crucial for activity, accordingly, future studies should focus on maximising the ability of ligands to (i) coordinate to the zinc rather than the iron and (ii) facilitate the formation of mixed (PP)Zn-Fe intermediates. Importantly, competition between the transition metal centre and the zinc reagent may not be limited to iron catalysts alone, and should be considered as a possibility in all transition metal-catalysed Negishi cross-coupling reactions.

Acknowledgements

We thank the following for support of the project: UK Catalysis Hub for resources and support provided *via* our membership of the UK Catalysis Hub Consortium and funded by EPSRC (grants EP/K014706/2, EP/K014668/1, EP/K014854/1, EP/K014714/1 and EP/M013219/1); EPSRC for funding (Grant no. EP/K012258/1), the provision of a studentship through the EPSRC Centre for Doctoral Training in Catalysis (S.L.J.L) and for a part-studentship (H.M.O'B.); AstraZeneca for CASE top-up funding (H.M.O'B.) and CONACYT (studentship for OHF). We thank Dr Natalie Fey for provision of and discussions concerning Ligand Knowledge Base data and Mr Paul Lawrence for help with setting up NMR experiments.

Author contributions

A.M.M., S.L.J.L., D.G., E.K.G., H.M.O'B., H.A.S., S.A.D., J.C., D.E., O.H.F., and R.B.B. performed experiments and analysed experiments. A.M.M. and P.P.W. designed the flow-XAFS cell. P.P.W., A.M.M., D.G., E.K.G., J.C. designed XAFS experiments. A.M.M., S.L.J.L., and R.B.B. designed synthetic and mechanistic experiments. R.B.B. designed computational experiments. R.B.B., A.M.M., P.P.W and S.L.J.L. prepared this manuscript.

Additional information

Full experimental methods and compound characterisation data are provided online in the Supplementary Information. Correspondence and requests for materials should be addressed to R.B.B.

Competing financial interests

The authors declare no competing financial interests.

Data availability:

Crystal structure data have been deposited at the Cambridge Crystallographic Data Centre (CCDC nos: 1836928-1836960 and 1868985) and crystallographic data are provided in the Supplementary Information. The spectroscopic, mass spectrometric, TEM and kinetic data that support the findings of this study are freely available in the University of Bristol data repository, data.bris, with the identifier https://doi.org/10.5523/bris.1kp2f62x3klb02mfz2qymcmxmx.

References

1. Johansson Seechurn, C. C. C., Kitching, M. O., Colacot, T. J. & Snieckus, V. Palladium-Catalyzed Cross-Coupling: A Historical Contextual Perspective to the 2010 Nobel Prize. *Angew. Chem. Int. Ed.* **51**, 5062 – 5085 (2012).

2. Nakamura, E., Hatakeyama, T., Ito, S., Ishizuka, K., Ilies, L. & Nakamura, M. Iron-Catalyzed Cross-Coupling Reactions, *Org. React.*, **83**, 1-210 (2014).

3. Bedford, R. B. & Brenner, P. B. The Development of Iron Catalysts for Cross-Coupling Reactions. *Top. Organomet. Chem*., **50**, 19-46 (2015).

4. Bauer, I. & Knölker, H.-J. Iron Catalysis in Organic Synthesis. *Chem. Rev.*, **115**, 3170–3387 (2015).

5. Bedford, R. B. How Low Does Iron Go? Chasing the Active Species in Fe-Catalyzed Cross-Coupling Reactions. *Acc. Chem. Res.*, **48**, 1485−1493 (2015).

6. Cassani, C., Bergonzini, G & Wallentin, C.-J. Active Species and Mechanistic Pathways in Iron-Catalyzed C−C Bond-Forming Cross-Coupling Reactions. *ACS Catal.*, **6**, 1640−1648 (2016).

7. Mako, T. L. & Byers, J. A. Recent advances in iron-catalysed cross coupling reactions and their mechanistic underpinning. *Inorg. Chem. Front.* **3**, 766–790 (2016).

8. Parchomyk, T. & Koszinowski, K. Iron-Catalyzed Cross-Coupling: Mechanistic Insight for Rational Applications in Synthesis. *Synthesis* **49**, 3269-3280 (2017).

9. Bedford, R. B., Betham, M., Bruce, D. W., Danopoulos, A. A., Frost, R. M. & Hird M. Iron-phosphine, -phosphite, -arsine, and -carbene catalysts for the coupling of primary and second- ary alkyl halides with aryl Grignard reagents*. J. Org. Chem.* **71**, 1104–1110 (2006).

10. Dongol, K. G., Koh, H., Sau, M. & Chai, C. L. L. Iron-catalysed sp^3–sp^3 cross-coupling reactions of unactivated alkyl halides with alkyl Grignard reagents. *Adv. Synth. Catal.* **349**, 1015–1018 (2007).

11. Bedford, R. B., Huwe, M. & Wilkinson, M. C. Iron-catalysed Negishi coupling of benzyl halides and phosphates. *Chem. Commun.* 600–602 (2009).

12. Hatakeyama, T., Kondo, Y., Fujiwara, Y. I., Takaya, H., Ito, S., Nakamura, E. & Nakamura, M. Iron-catalysed fluoroaromatic coupling reactions under catalytic modulation with 1,2-bis (diphenylphosphino)benzene. *Chem. Commun.* 1216–1218 (2009).

13. Bedford, R. B., Hall, M. A., Hodges, G. R., Huwe, M. & Wilkinson, M. C. Simple mixed Fe-Zn catalysts for the Suzuki couplings of tetraarylborates with benzyl halides and 2-halopyridines. *Chem. Commun.* 6430–6432 (2009).

14. Kawamura, S., Ishizuka, K., Takaya, H. & Nakamura, M. The first iron-catalysed aluminium-variant Negishi coupling: critical effect of co-existing salts on the dynamic equilibrium of arylaluminium species and their reactivity. *Chem. Commun.* **46**, 6054–6056 (2010).

15. Hatakeyama, T., Hashimoto, T., Kondo, Y., Fujiwara, Y., Seike, H., Takaya, H., Tamada, Y., Ono, T. & Nakamura, M. Iron-catalyzed Suzuki-Miyaura coupling of alkyl halides. *J. Am. Chem. Soc.* **132**, 10674–10676 (2010).

16. Hatakeyama, T., Fujiwara, Y., Okada, Y., Itoh, T., Hashimoto, T., Kawamura, S., Ogata. K., Takaya, H. & Nakamura, M. Kumada-Tamao-Corriu coupling of alkyl halides catalyzed by an iron-bisphosphine complex. *Chem. Lett.* **40**, 1030–1032 (2011).

17. Hatakeyama, T., Okada, Y., Yoshimoto, Y. & Nakamura, M. Tuning chemoselectivity in iron-catalyzed Sonogashira-type reactions using a bisphosphine ligand with peripheral steric bulk: selective alkynylation of nonactivated alkyl halides. *Angew. Chem. Int. Ed.* **50**, 10973–10976 (2011).

18. Lin, X., Zheng, F. & Qing, F.-L. Iron-catalyzed cross-coupling reactions between arylzinc reagents and alkyl halides bearing β-fluorines. *Organometallics* **31**, 1578–1582 (2012).

19. Kawamura, S., Kawabata, T., Ishizuka, K. & Nakamura, M. Iron-catalysed cross-coupling of halohydrins with aryl aluminium reagents: a protecting-group-free strategy attaining remarkable rate enhancement and diastereoinduction. *Chem. Commun.* **48**, 9376–9378 (2012).

20. Hashimoto, T., Hatakeyama, T. & Nakamura, M. Stereospecific cross-coupling between alkenylboronates and alkyl halides catalyzed by iron–bisphosphine complexes. *J. Org. Chem.* **77**, 1168–1173 (2012).

21. Hatakeyama, T., Hashimoto, T., Kathriarachchi, K., Zenmyo, T., Seike, H. & Nakamura, M. Iron-catalyzed alkyl-alkyl Suzuki-Miyaura coupling. *Angew. Chem. Int. Ed.* **51**, 8834–8837 (2012).

22. Adams, C. J., Bedford, R. B., Carter, E., Gower, N. J., Haddow, M. F., Harvey. J. N., Huwe, M., Cartes, M. A., Mansell, S. M., Mendoza, C., Murphy, D. M., Neeve, E. C. & Nunn, J. Iron(I) in Negishi cross-coupling reactions. *J. Am. Chem. Soc.* **134**, 10333–10336 (2012).

23. Kawamura, S. & Nakamura, M. Ligand-controlled iron-catalyzed cross coupling of benzylic chlorides with aryl Grignard reagents. *Chem. Lett.* **42**, 183–185 (2013).

24. Bedford, R. B., Carter, E., Cogswell, P. M., Gower, N. J., Haddow, M. F., Harvey, J. N., Murphy, D. M., Neeve, E. C. & Nunn, J. Simplifying iron-phosphine catalysts for cross-coupling reactions. *Angew. Chem. Int. Ed.* **52**, 1285–1288 (2013).

25. Sun, C.-L., Krause, H. & Fürstner, A. A practical procedure for iron-catalyzed cross-coupling reactions of sterically hindered aryl-Grignard reagents with primary alkyl halides. *Adv. Synth. Catal.* **356**, 1281–1291 (2014).

26. Bedford, R. B., Brenner, P. B., Carter, E., Clifton, J., Cogswell, P. M., Gower, N. J., Haddow, M. F., Harvey, J. N., Kehl, J. A., Murphy, D. M., Neeve, E. C., Neidig, M. L., Nunn, J., Snyder, B. E. R. & Taylor, J. Iron phosphine catalyzed cross-coupling of tetraorganoborates and related Group 13 nucleophiles with alkyl halides. *Organometallics* **33**, 5767–5780 (2014).

27. Bedford, R. B., Brenner, P. B., Carter, E., Carvell, T. W., Cogswell, P. M., Gallagher, T., Harvey, J. N., Murphy, D. M., Neeve, E. C., Nunn, J. & Pye, D. R. Expedient iron-catalyzed coupling of alkyl, benzyl and allyl halides with arylboronic esters. *Chem. Eur. J.* **20**, 7935–7938 (2014).

28. Clifton, J., Habraken, E. R. M., Pringle, P. G. & Manners, I. *Catal. Sci. Technol.* **5**, 4350–4353 (2015).

29. Daifuku, S. L., Al-Afyouni, M. H., Snyder, B. E. R., Kneebone, J. L. & Neidig, M. L. A Combined Mössbauer, Magnetic Circular Dichroism, and Density Functional Theory Approach for Iron Cross-Coupling Catalysis: Electronic Structure, In Situ Formation, and Reactivity of Iron- Mesityl-Bisphosphines. *J. Am. Chem. Soc.* **136**, 9132−9143 (2014).

30. Daifuku, S. L., Kneebone, J. L., Snyder, B. E. R. & Neidig, M. L. Iron(II) Active Species in Iron−Bisphosphine Catalyzed Kumada and Suzuki−Miyaura Cross-Couplings of Phenyl Nucleophiles and Secondary Alkyl Halides. *J. Am. Chem. Soc.* **137**, 11432−11444 (2015).

31. Falivene, L.; Credendino, R.; Poater, A.; Petta, A.; Serra, L.; Oliva, R.; Scarano, V. & Cavallo, L. SambVca 2. A Web Tool for Analyzing Catalytic Pockets with Topographic Steric Maps. *Organometallics* **35**, 2286−2293 (2016).

32. Lovitt, C.F.; Frenking, G. & Girolami, G.S. Donor−Acceptor Properties of Bidentate Phosphines. DFT Study of Nickel Carbonyls and Molecular Dihydrogen Complexes. *Organometallics* **31**, 4122−4132 (2012).

33. Jover, J. and Fey, N. Screening substituent and backbone effects on the properties of bidentate P,P-donor ligands (LKB-PP_{screen}). *Dalton Trans*. **42**, 172–181 (2013).

34. Takaya, H., Nakajima, S., Nakagawa, N., Isozaki, K., Iwamoto, T., Imayoshi, R., Gower, N. J., Adak, L., Hatakeyama, T., Honma, T., Takagaki, M., Sunada, Y., Nagashima, H., Hashizume, D., Takahashi, O. & Nakamura, M. Investigation of Organoiron Catalysis in Kumada-Tamao-Corriu-Type Cross-Coupling Reaction Assisted by Solution-Phase X-ray Absorption Spectroscopy. *Bull. Chem. Soc. Jpn.* **88**, 410–418 (2015).

35. Langer, R. Bönisch, F., Maser, L. Pietzonka, C., Vondung, L. & Zimmermann, T. P. Substitutional Lability of Diphosphine Ligands in Tetrahedral Iron(II) Chloro Complexes. *Eur. J. Inorg. Chem*. 141-148 (2015).

36. Barclay, J. E., Hills, A., Hughes, D. L. & Leigh, G. J. Crystal and Molecular Structures of Four Bis(diphosphine) Complexes of Iron(II): Bis[1.2-bis(diethylphosphino)ethane]di-iodoiron(II), Dichlorobis[*o*-phenylenebis(diphenylphosphine)]iron(II), Bis(acetonitrile)bis[*o*-phenylenebis(diphenylphosphine)]iron(II)Di-iodide, and Iodobis-[*o*-phenylenebis(diphenylphosphine)]iron(II) Iodide. *J. Chem. Soc., Dalton Trans.* 2871-2877 (1988).

37. Evans, D. J., Henderson, R. A., Hills, A., Hughes, D. L. & Oglieve, K. E. Involvement of Iron Alkyl Complexes and Alkyl Radicals in the Kharasch Reactions: Probing the Catalysis using Iron Phosphine Complexes. *J. Chem. Soc. Dalton Trans.* 1259-1265 (1992).

38. Wu, C.-C. Jung, J., Gantzel, P. K., Gütlich, P. & Hendrickson, D. N. LIESST Effect Studies of Iron(II) Spin-Crossover Complexes with Phosphine Ligands: Relaxation Kinetics and Effects of Solvent Molecules. *Inorg. Chem.* **36**, 5339-5347 (1997).

39. Schoch, R., Desens, W,. Werner, T. & Bauer, M. X-ray Spectroscopic Verification of the Active Species in Iron-Catalyzed Cross-Coupling Reactions. *Chem. Eur. J.* **19**, 15816 – 15821 (2013).

40. Welther, A., Bauer, M., Mayer, M. & Jacobi von Wangelin Iron(0) Particles: Catalytic Hydrogenations and Spectroscopic Studies. *ChemCatChem* **4**, 1088 – 1093 (2012).

41. Bedford, R. B., Betham, M., Bruce, D. W., Davis, S. A., Frost, R. M. & Hird, M. Iron nanoparticles in the coupling of alkyl halides with aryl Grignard reagents. *Chem. Commun.*, 1398–1400 (2006).

42. Bedford, R. B., Brenner, P. B., Carter, E., Cogswell, P. M., Haddow, M. F., Harvey, J. N., Murphy, D. M., Nunn, J. & Woodall, C. H. TMEDA in Iron-Catalyzed Kumada Coupling: Amine Adduct versus Homoleptic “ate” Complex Formation. *Angew. Chem. Int. Ed.*, **53**, 1804 –1808 (2014).

43. Klose, A., Solari, E., Floriani, C., Chiesi-Villa, A., Rizzoli, C. & Re, N. Magnetic Properties Diagnostic for the Existence of Iron(II)-Iron(II) Bonds in Dinuclear Complexes Which Derive from Stepwise Insertion Reactions on Unsupported Iron-Aryl Bonds. *J. Am. Chem. Soc.*, **116**, 9123-9135 (1994).

44. Jefferis, J. M., & Girolami, G. S. Crystal Structure of “$[Li(Et_2O)]_4[FePh_4]$”: Corrigendum and Reformulation. A Remarkable Example of a False Solution in a Wrong Space Group *Organometallics* **17**, 3630-3632 (1998).

45. Huang, F., Yao, Z.-K., Wang, Y., Wang, Y., Zhang, J. & Yu, Z.-X. C-H Bond Activation/Borylation of Furans and Thiophenes Catalyzed by a Half-Sandwich Iron *N*-Heterocyclic Carbene Complex. *Chem. Asian J.* **5**, 1657-1666 (2010).

46. Kalman, S. E. Petit, A., Gunnoe, T. B., Ess, D. H., Cundari, T. R. & Sabat, M. Facile and Regioselective C−H Bond Activation of Aromatic Substrates by an Fe(II) Complex Involving a Spin-Forbidden Pathway. Organometallics **32**, 1797-1806 (2013).

47. Goedken, V. L. Peng, S.-M. & Park, Y. A New Route to the Formation of Organocobalt(III) and Organoiron(III) Complexes. Alkylation *via* Oxidative Deamination of Organic Hydrazines. *J. Am. Chem. Soc.* **96**, 284-285 (1974).

48. Sciarone, T. J. J., Meetsma, A., Hesssen, B. & Teuben, J. H. Benzyl anion abstraction from a (β-diiminato)Fe(II) benzyl complex. *Chem. Commun.* 1580-1581 (2002).

49. Mund,G., Vidovic, D., Batchelor, R. J., Britten, J. F., Sharma, R. D., Jones, C. H. W. & Leznoff, D. B. Unusual Iron(III) Ate Complexes Stabilized By Li–π Interactions. *Chem. Eur. J.* **9**, 4757-4763 (2003).

50. Rose, R. P., Jones, C., Schulten, C., Aldridge, S. & Stasch, A. Synthesis and Characterization of Amidinate–Iron(I) Complexes: Analogies with β-Diketiminate Chemistry. *Chem. Eur. J.* **14**, 8477-8480 (2008).

51. Taherimehr, M., Al-Amsyar, S. M., Whiteoak, C. J., Kleij, A. W. & Pescarmona, P. P. High activity and switchable selectivity in the synthesis of cyclic and polymeric cyclohexene carbonates with iron amino triphenolate catalysts. *Green Chem.* **15**, 3083-3090 (2013).

52. Lichtenberg, C., Adelhardt, M., Wörle, M., Büttner, T., Meyer, K. & Grützmacher, H. Mono- and Dinuclear Neutral and Cationic Iron(II) Compounds Supported by an Amidinato-diolefin Ligand: Characterization and Catalytic Application. *Organometallics* **34**, 3079-3089 (2015).

53. Trovitch, R. J., Lobkovsky, E. & Chirik, P. J. Bis(imino)pyridine Iron Alkyls Containing β-Hydrogens: Synthesis, Evaluation of Kinetic Stability, and Decomposition Pathways Involving Chelate Participation *J. Am. Chem. Soc.* **130**, 11631-11640 (2008).

54. Ouyang, Z., Du, J. Wang, L., Kneebone, J. L., Neidig, M. L. & Deng, L. Linear and T-Shaped Iron(I) Complexes Supported by N-Heterocyclic Carbene Ligands: Synthesis and Structure Characterization. *Inorg. Chem.* **54**, 8808-8816 (2015).

55. Ohki, Y., Hoshino, R. & Tatsumi, K. N-Heterocyclic Carbene Complexes of Three- and Four-Coordinate Fe(I). *Organometallics* **35**, 1368-1375 (2016)

56. Tromp, M., Moulin, J., Reid, G. & Evans, J. Cr K-Edge XANES Spectroscopy: Ligand and Oxidation State Dependence — What is Oxidation State? *AIP Conference Proceedings* **882**, 699-701 (2007).

57. Liu, X., Liu, Y., Hao, Y., Yang, X.-J. & Wu, B. Square helix versus zigzag chain of group 12 metal coordination polymers with 1,2-bis(diphenylphosphino)ethane (dppe). *Inorg. Chem. Comm.* **13**, 511–513 (2010).

58. Dunsford, J. J, Clark, E. R. & Ingleson, M. J. Direct C(sp^2)-C(sp^3) Cross-Coupling of Diaryl Zinc Reagents with Benzylic, Primary, Secondary,and Tertiary Alkyl Halides. *Angew. Chem. Int. Ed.* **54**, 5688 –5692 (2015).

59. Abbenhuis, H. C. L., Feiken, N., Haarman, H. F., Grove,D. M., Horn, E., Spek, A. L., Pfeffer, M. & van Koten, G. A Bimetallic Tantalum-Zinc Complex with an Ancillary Aryldiamine Ligand as Precursor for a Reactive Alkylidyne Species: Alkylidyne-Mediated C-H Activation and a Palladium-Mediated Alkylidyne Functionalization. Organomietallics **12**, 2227-2235 (1993).

60. Liberman-Martin, A. L., Levine, D. S., Ziegler, M. S., Bergman, R. G. & Tilley, T. D. Lewis acid–base interactions between platinum(II) diaryl complexes and bis(perfluorophenyl)zinc: strongly accelerated reductive elimination induced by a Z-type ligand. *Chem. Commun.* **52**, 7039-7042 (2016).

61. Garden, J. A., White, A. J. P. & Williams, C. K. Heterodinuclear titanium/zinc catalysis: synthesis, characterization and activity for CO_2/epoxide copolymerization and cyclic ester polymerization. *Dalton Trans.* **46**, 2532-2541 (2017).